A Spatially Localized Architecture for Fast and Modular Computation at the Molecular Scale

Gourab Chatterjee[1], Neil Dalchau[2], Richard A. Muscat[3], Andrew Phillips[2*], Georg Seelig[3,4*]

[1]Department of Bioengineering, University of Washington, Seattle, WA 98195, USA

[2]Microsoft Research, Cambridge CB1 2FB, UK

[3]Department of Electrical Engineering, University of Washington, Seattle, WA 98195, USA

[4]Department of Computer Science & Engineering, University of Washington, Seattle, WA 98195, USA

*To whom correspondence should be addressed;
E-mail: gseelig@uw.edu or andrew.phillips@microsoft.com

1 **Cells use spatial constraints to control and accelerate the flow of information in enzyme cas-**
2 **cades and signaling networks. Here we show that spatial organization can be a similarly**
3 **powerful design principle for overcoming limitations of speed and modularity in engineered**
4 **molecular circuits. We create logic gates and signal transmission lines by spatially arranging**
5 **reactive DNA hairpins on a DNA origami. Signal propagation is demonstrated across trans-**
6 **mission lines of different lengths and orientations, and logic gates are modularly combined**
7 **into circuits that establish the universality of our approach. Because reactions preferen-**
8 **tially occur between neighbors, identical DNA hairpins can be reused across circuits. Co-**
9 **localization of circuit elements decreases computation time from hours to minutes compared**
10 **to circuits with diffusible components. Detailed computational models enable predictive cir-**
11 **cuit design. We anticipate that our approach will motivate the use of spatial constraints in**
12 **molecular engineering more broadly, bringing embedded molecular control circuits closer to**

applications.

Human-engineered systems, from ancient irrigation networks to modern semiconductor circuitry, rely on spatial constraints to guide the flux of materials and information. Cells similarly use spatial organization, through enzyme scaffolds, organelles and chaperones, to perform complex information processing tasks within a crowded intracellular environment. Such spatial constraints play a pivotal role, by accelerating interactions between components that are closer together, and reducing interference between those that are further apart. Not surprisingly, spatial organization has been recognized as a potentially powerful engineering principle for the construction of synthetic molecular circuitry. However, in practice, synthetic circuits have so far relied almost exclusively on interactions between diffusible components guided by chemical specificity[1–3]. As a result, scaling up such circuits for complex and parallel computation rapidly becomes intractable, due to the limited availability of orthogonal components. Here, we demonstrate a novel design paradigm for realizing scalable molecular logic circuits with a minimal set of orthogonal components, using spatial organization rather than sequence specificity as the main organizing principle.

DNA nanotechnology provides an ideal framework for exploring the use of spatial constraints in molecular circuit design. First, DNA origami forms a uniquely programmable scaffold for the controlled arrangement of molecular circuit elements[8]. Second, research on DNA-based walking motors corroborates the notion that programmed, multi-step reactions can occur in DNA systems with spatial constraints. Over the last decade such DNA walking motors, mainly powered by enzyme catalysis, have progressed from being able to make a small number of externally triggered steps to autonomously moving along multi-step tracks laid out on a DNA origami[9–12]. Walking motors could in principle be programmed to perform computation[13–15]. However, by considering that only information needs to propagate in a computational circuit, rather than a specific motor molecule, we open up a much broader design space for engineering. Third, DNA strand displacement[16,17] provides a mechanism for the rational design of complex digital[4,18] and ana-

38 log circuits[19, 20], neural networks[21, 22] and reaction diffusion patterns[23, 24], with quantitatively pre-

39 dictable behaviors. Such DNA strand displacement circuits form a benchmark for success, but also

40 pose a set of challenges that need to be overcome through novel design approaches. In particu-

41 lar, circuit operation is slow at experimentally realistic concentrations. Furthermore, unintentional

42 binding interactions between sequences degrade performance and increase with circuit size, lead-

43 ing to a lack of modularity in circuit design and execution.

44   Several theoretical papers have proposed DNA circuit architectures that take advantage of

45 spatial constraints to overcome these limitations of speed and modularity[25–28]. Limiting interac-

46 tions to spatially proximal circuit elements should result in faster reactions, since spatial localiza-

47 tion allows the effective concentrations of components to be substantially increased, compared to

48 components in solution. Moreover, sequences can be reused across components because proximity

49 rather than chemical specificity controls information flow. Recent experimental work has begun

50 to characterize the kinetics of strand displacement reactions with localized components, providing

51 evidence for an increase in circuit speed due to localization[29–31], and elementary localized DNA

52 logic gates have also been built[32, 33]. However, an experimental realization of a scalable circuit

53 architecture that exploits the advantages of spatial organization is still lacking.

54   Here we experimentally demonstrate a modular design strategy – the "DNA domino" archi-

55 tecture – that uses spatial organization to realize fast arbitrary logic at the molecular scale. Domino

56 gates and signal transmission lines (wires) are realized with DNA hairpins laid out on a DNA

57 origami scaffold (Fig. 1a, Supplementary Fig. S1). The reaction mechanism underlying circuit

58 operation reimagines the hybridization chain reaction (HCR)[34], such that polymerization occurs

59 along designed trajectories on an origami[25]. All reactions are rationally designed and, unlike most

60 DNA walking motors, no enzyme or ribozyme catalysis is required for operation.

Localized signal propagation mechanism

To illustrate how information is propagated spatially, we consider the "DNA domino effect" in a minimal two-hairpin wire comprised of an Input and Output hairpin attached to a DNA origami scaffold (Fig. 1b). In each reaction step, a hairpin stem is unwound and a toehold that is initially sequestered in the hairpin loop becomes available, to initiate the unwinding of a subsequent hairpin stem. The Input hairpin is opened by binding of an input strand, which enables the capture of a diffusible Fuel hairpin. Requiring a diffusible Fuel ensures that no unwanted reactions can occur between Input and Output hairpins during initial assembly of the origami. In practice, the Fuel can be added in large excess over the concentrations of the other components, and thus does not substantially limit reaction speed. The Output hairpin is opened by the Fuel-bound Input hairpin via a fast local interaction. Finally, the activated Output hairpin displaces the quencher-labeled strand from the diffusible Reporter complex, resulting in increased Reporter fluorescence.

To demonstrate the benefits of spatial organization, we experimentally compared signal propagation between Input and Output hairpins, positioned at different distances from each other or on different scaffolds (Fig. 1c). We first confirmed that a signal could rapidly propagate across proximally positioned Input and Output hairpins (single spacing) in a two-hairpin wire ($t_{1/2} <$ 3 mins). No observable signal transfer was observed without input addition. We then doubled the distance between Input and Output hairpins (double spacing) on the same origami, and showed that separating the hairpins beyond their theoretical maximum reach resulted in minimal signal transfer (Fig. 1c, Supplementary Fig. S4). Furthermore, we found that interactions between Input and Output hairpins on two different origamis were significantly slower than single-spaced hairpin interactions on the same origami, and comparable to the double-spaced hairpin interactions. Crucially, decreasing the operating concentration of the origamis did not affect the speed of localized intra-origami signal propagation, but significantly reduced the speed of non-localized inter-origami interactions (Supplementary Fig. S5).

86 We quantified the kinetics of domino circuits by constructing detailed computational models

87 and parameterizing them using experimental data (Supplementary Figures S6 - S18). Interactions

88 involving a diffusible molecule and a tethered hairpin were modelled as bimolecular reactions ac-

89 cording to mass action kinetics, while interactions between two complexes tethered to the same

90 origami were converted to unimolecular reactions by scaling with a *local concentration*[27,35,36]. We

91 used parameter inference techniques to establish a maximum likelihood parameter set (Supplemen-

92 tary Fig. S15). By ensuring that equivalent interactions in different circuits were parameterized

93 with the same rate constants, we were able to demonstrate consistency in the quantitative behavior

94 of our circuits. In this way, models were used throughout this study for the design and optimization

95 of circuit behavior.

Signal propagation through molecular wires

97 We created wires of varying lengths and orientations (Supplementary Fig. S1 and Fig. S19) to

98 allow signal propagation over extended distances, by using Intermediate hairpins (Supplementary

99 Fig. S20) as signal relaying components. Multiple identical Intermediate hairpins were positioned

100 at appropriate distances (single spacing) to relay the signal from an Input to an Output hairpin. A

101 schematic of an untriggered eight hairpin domino wire is shown in Fig. 2a. We experimentally ob-

102 served fast and reliable signal propagation through wires with up to 8 hairpins (spanning over 80

103 nm) along the origami helical axis ($t_{1/2} < 10$ mins.; Fig. 2b), with up to 4 hairpins perpendicular

104 to this axis ($t_{1/2} < 6$ mins.; Fig. 2c), and with up to 7 hairpins through a 180 degree turn ($t_{1/2} < 10$

105 mins.; Fig. 2d). We observed significantly reduced signal propagation whenever an Intermediate

106 hairpin was intentionally omitted, and found that signals propagated preferentially via neighbour-

107 ing hairpins (Supplementary Fig. S21). Signal completion levels varied approximately inversely

108 with track length (Supplementary Fig. S22, Fig. S23), likely due to imperfect incorporation of

109 hairpins into the origami (Supplementary Fig. S24). The non-monotonic decrease in signal can

110 be explained by position-dependent hairpin incorporation efficiency (Supplementary Fig. S25).

[111] Signal production due to inter-origami interactions increased with the number of hairpins, but even [112] for an eight-hairpin wire was considerably lower than signal production through localized interac- [113] tions. As noted previously, lowering the origami concentrations significantly reduced inter-origami [114] interactions, with minimal effect on the speed of localized signal propagation (Supplementary Fig. [115] S26, S27).

Design and construction of elementary logic gates

[117] As a prerequisite for performing arbitrary logic computation with our domino architecture, we [118] next designed two-input OR and AND gates. The two-input OR domino gate was implemented [119] through a wire fan-in by positioning an Output hairpin close to two orthogonal Input hairpins [120] on the origami (Fig. 3a). Because all hairpin components were constrained to have the same [121] stem, input orthogonality was ensured by using distinct toehold sequences. Experimentally, no [122] significant output fluorescence was observed in absence of both Inputs, but addition of either one [123] or both Inputs resulted in high output fluorescence, consistent with OR logic ($t_{1/2} < 5$ mins).

[124] To implement a two-input AND domino gate, we used a thresholding strategy to prevent [125] signal propagation when only one of the inputs is present. Specifically, a "Threshold hairpin" [126] was designed to block signal propagation by outcompeting the Output hairpin. We ensured pref- [127] erential binding to the Threshold hairpin by shortening the Output hairpin toehold, while keeping [128] the Threshold hairpin toehold at 6 nucleotides (Fig. 3b and Supplementary Fig. S28). Once the [129] Threshold hairpin is opened, it captures a partially double-stranded "Threshold block", making [130] signal inhibition practically irreversible. Experimentally, the extent of preferential binding to the [131] Threshold hairpin depended on the difference in toehold lengths (Fig. 3b), where a 3 nucleotide [132] Output hairpin toehold was found to be optimal. Consequently, all domino logic circuits presented [133] in this study, including the OR gate discussed above, were constructed using Input and Thresh- [134] old hairpins with 6 nucleotide toeholds, and Intermediate and Output hairpins with 3 nucleotide

135 toeholds.

136 The two-input AND domino gate was implemented by combining an OR gate with a Thresh-
137 old hairpin. The Output and Threshold hairpins were positioned at equal distances to two or-
138 thogonal Input hairpins (Fig. 3c). When only one of the input strands is added, the Threshold
139 hairpin blocks signal propagation, resulting in low output fluorescence. When both input strands
140 are added, the signal from one of the inputs is blocked, while the signal from the other input suc-
141 cessfully propagates to the Output hairpin and generates high output fluorescence ($t_{1/2} < 6$ mins.),
142 consistent with two-input AND logic.

143 The measurements of the two-input OR, threshold and two-input AND gates were included
144 in the parametrization of our computational models. Kinetic parameters for input and fuel binding
145 were shared between all circuits. However, we used distinct local concentration parameters for
146 the wires and logic circuits, since the spacing between hairpins was slightly different in these two
147 settings. The ratio between the binding rates of the Threshold and the Output hairpin was also
148 calibrated to the experimental data, and was approximately 10 to 1 (Supplementary Fig. S15).
149 The simulated model behaviors were consistent with the measured kinetics for the two-input OR,
150 threshold and two-input AND gates (Fig. 3 and Supplementary Fig. S16).

Modular cascading of logic gates to build complex logic circuits

152 To demonstrate modular circuit design using our domino architecture, we built a three-input AND
153 gate by cascading a pair of two-input AND gates on the same origami. Specifically, we replaced
154 the Output hairpin of an upstream two-input AND gate with an Intermediate hairpin, such that
155 the output of the first gate was relayed to the input of the second (Fig. 4a and Supplementary
156 Fig. S29). Upon addition of any combination of two input strands, the circuit showed low output
157 fluorescence. When all three input strands were added there was high output fluorescence ($t_{1/2} <$
158 6 mins.), consistent with three-input AND logic. Furthermore, the experimental data exhibited

7

159 the expected Boolean logic. We were able to quantitatively predict the dynamics of the three-
160 input AND gate through model simulation, using the parameters obtained from our previously
161 characterized circuits (Fig. 4a).

162   Next, we positioned two distinct three-input AND gates side by side and triggered them
163 simultaneously, to determine whether multiple circuits on the same origami can function concur-
164 rently (Fig. 4b). Both gates used the same Intermediate and Threshold hairpins throughout, along
165 with the universal Fuel, but used distinct toeholds for the Input and Output hairpins to ensure
166 orthogonality. Experimental measurements were consistent with model predictions (Fig. 4b).

167   To further demonstrate scalability, we constructed a six-input AND gate by connecting the
168 outputs of both three-input AND gates, using an additional two-input AND gate (Fig. 4c and
169 Supplementary Fig. S30). When all six inputs were added the circuit produced high output signal
170 ($t_{1/2}$ ~12 mins.). Conversely, the circuit produced low output for any combination of five or fewer
171 inputs. While the number of hairpins increased from four for the two-input AND gate, to eighteen
172 for the six-input AND gate, all hairpins used the same conserved set of only five domains, plus
173 a separate domain for each input and output. Similar to our experiments on wires, we observed
174 attenuation of the output signal with increasing number of hairpins (Supplementary Fig. S23).
175 This signal loss can in part be explained with a model assuming a fixed non-zero probability of
176 hairpin omission (Supplementary Fig. S24).

177   To exemplify arbitrary Boolean logic computation using our domino architecture, we built a
178 two-input dual-rail XNOR gate (Fig. 4d and Supplementary Fig. S31). Dual-rail encoding allows
179 an arbitrary Boolean logic function to be realized using only a combination of AND and OR gates,
180 avoiding the need for NOT gates, which are difficult to implement experimentally[4]. Each input
181 variable A is specified as TRUE by a dedicated signal strand A1, and specified as FALSE by a
182 distinct signal strand A0 (Fig. 4d). Only one of the two strands is present at any given time.

8

Accordingly, our dual rail XNOR gate was implemented as a pair of parallel circuits, computing TRUE and FALSE outputs separately. The complete circuit arranged seventeen hairpins into six two-input AND and OR gates. The experimental data showed signal propagation ($t_{1/2} < 8$ mins.) consistent with predictions from the computational model.

Discussion

Overall, the number of unique sequences required for building any complex domino circuit did not depend on the number of constituent gates, but only on the number of inputs and outputs. Our domino circuits also performed significantly faster than previous systems with diffusible components (Supplementary Table S2). For example, a three-input AND domino gate had a half time of 7 min with operating concentration of only 2 nM, compared to 4 hours for an equivalent non-localized circuit with diffusible components operated at 100 nM concentration [4].

The modularity of our design approach enabled us to construct a family of cascaded circuits spanning an entire rectangular tile origami. Even larger and more complex circuit designs could be made with bigger and multilayered stiffer origami scaffolds, however three issues would need to be addressed. First, inputs are currently distinguished only by their toehold domains, and in practice the number of sufficiently orthogonal six nucleotide toeholds is small. This limitation can be overcome by incorporating an additional recognition domain in the Input hairpin, to encode input specificity (Supplementary Fig. S32). Second, we observed signal attenuation with increasing circuit size, likely due to imperfect hairpin incorporation. Such imperfections will become less limiting with continuing improvements in origami assembly protocols. Alternatively, component redundancy could be used to compensate for assembly defects, and signal restoration modules could overcome attenuation. Third, although inter-origami interactions are not currently limiting, they could become significant as circuit size increases. Such interactions could be minimized by using immobilizing techniques to tether origami molecules to a surface, or by using closed

3-dimensional origamis with components tethered to the inner faces.

Circuit architectures with localized components may provide a path towards the delivery of DNA circuits to cells, a long-held ambition of dynamic DNA nanotechnology that only recently started to become reality[37–39]. Not only do localized circuits enable control of stoichiometry during delivery, but increased speed compared to non-localized circuits may be even more pronounced in the densely packed cellular environment. Moreover, localized circuits could be used to increase the complexity of chemical synthesis reactions achievable with DNA-templated chemistry[40,41] or to enhance the specificity of theranostic DNA robots[42].

References

1. Polka, J. K., Hays, S. G. & Silver, P. A. Building spatial synthetic biology with compartments, scaffolds, and communities. *Cold Spring Harbor Perspectives in Biology* **8** (2016).

2. Park, S.-H., Zarrinpar, A. & Lim, W. A. Rewiring MAP kinase pathways using alternative scaffold assembly mechanisms. *Science (New York, N.Y.)* **299**, 1061–1064 (2003).

3. Delebecque, C. J., Lindner, A. B., Silver, P. A. & Aldaye, F. A. Organization of intracellular reactions with rationally designed RNA assemblies. *Science (New York, N.Y.)* **333**, 470–474 (2011).

4. Qian, L. & Winfree, E. Scaling up digital circuit computation with DNA strand displacement cascades. *Science (New York, N.Y.)* **332**, 1196–201 (2011).

5. Xie, Z., Wroblewska, L., Prochazka, L., Weiss, R. & Benenson, Y. Multi-input RNAi-based logic circuit for identification of specific cancer cells. *Science (New York, N.Y.)* **333**, 1307–11 (2011).

229   6. Nielsen, A. A. K. *et al.* Genetic circuit design automation. *Science (New York, N.Y.)* **352**,
230   aac7341 (2016).

231   7. Purnick, P. E. M. & Weiss, R. The second wave of synthetic biology: from modules to systems.
232   *Nature reviews. Molecular cell biology* **10**, 410–22 (2009).

233   8. Rothemund, P. W. K. Folding DNA to create nanoscale shapes and patterns. *Nature* **440**,
234   297–302 (2006). `0202466`.

235   9. Wickham, S. F. J. *et al.* A DNA-based molecular motor that can navigate a network of tracks.
236   *Nature Nanotechnology* **7**, 169–73 (2012).

237   10. Muscat, R. A., Bath, J. & Turberfield, A. J. A programmable molecular robot. *Nano Letters*
238   **11**, 982–987 (2011).

239   11. Gu, H., Chao, J., Xiao, S.-J. & Seeman, N. C. A proximity-based programmable DNA
240   nanoscale assembly line. *Nature* **465**, 202–205 (2010).

241   12. Lund, K. *et al.* Molecular robots guided by prescriptive landscapes. *Nature* **465**, 206–10
242   (2010).

243   13. Boemo, M. A., Lucas, A. E., Turberfield, A. J. & Cardelli, L. The Formal Language and
244   Design Principles of Autonomous DNA Walker Circuits. *ACS Synthetic Biology* **5**, 878–884
245   (2016).

246   14. Dannenberg, F., Kwiatkowska, M. Z., Thachuk, C. & Turberfield, A. J. DNA walker circuits:
247   computational potential, design, and verification. *Natural Computing* **14**, 195–211 (2015).

248   15. Mo, D., Lakin, M. R. & Stefanovic, D. Scalable design of logic circuits using an active
249   molecular spider system. In *Lecture Notes in Computer Science*, vol. 9303, 13–28 (2015).

16. Yurke, B., Turberfield, a. J., Mills, a. P., Simmel, F. C. & Neumann, J. L. A DNA-fuelled molecular machine made of DNA. *Nature* **406**, 605–608 (2000).

17. Zhang, D. Y. & Seelig, G. Dynamic DNA nanotechnology using strand-displacement reactions. *Nature Chemistry* **3**, 103–113 (2011). `NIHMS150003`.

18. Seelig, G., Soloveichik, D., Zhang, D. Y. & Winfree, E. Enzyme-free nucleic acid logic circuits. *Science (New York, N.Y.)* **314**, 1585–8 (2006).

19. Soloveichik, D., Seelig, G. & Winfree, E. DNA as a universal substrate for chemical kinetics. *Proceedings of the National Academy of Sciences* **107**, 5393–5398 (2010).

20. Chen, Y.-J. *et al.* Programmable chemical controllers made from DNA. *Nature Nanotechnology* **8**, 755–62 (2013). `NIHMS150003`.

21. Qian, L., Winfree, E. & Bruck, J. Neural network computation with DNA strand displacement cascades. *Nature* **475**, 368–72 (2011).

22. Genot, A. J., Fujii, T. & Rondelez, Y. Scaling down DNA circuits with competitive neural networks. *Journal of the Royal Society, Interface / the Royal Society* **10**, 20130212 (2013).

23. Chirieleison, S. M., Allen, P. B., Simpson, Z. B., Ellington, A. D. & Chen, X. Pattern transformation with DNA circuits. *Nature chemistry* **5**, 1000–5 (2013).

24. Scalise, D. & Schulman, R. Designing modular reaction-diffusion programs for complex pattern formation. *Technology* **02**, 55–66 (2014).

25. Muscat, R. A., Strauss, K., Ceze, L. & Seelig, G. Dna-based molecular architecture with spatially localized components. *SIGARCH Comput. Archit. News* **41**, 177–188 (2013).

26. Chandran, H., Gopalkrishnan, N., Phillips, A. & Reif, J. H. Localized hybridization circuits. In *Lecture Notes in Computer Science*, vol. 6937, 64–83 (2011).

27. Dalchau, N., Chandran, H., Gopalkrishnan, N., Phillips, A. & Reif, J. Probabilistic Analysis of Localized DNA Hybridization Circuits. *ACS Synthetic Biology* **4**, 898–913 (2015).

28. Qian, L. & Winfree, E. Parallel and scalable computation and spatial dynamics with dna-based chemical reaction networks on a surface. In *Lecture Notes in Computer Science*, vol. 8727, 114–131 (2014).

29. Teichmann, M., Kopperger, E. & Simmel, F. C. Robustness of localized DNA strand displacement cascades. *ACS Nano* **8**, 8487–8496 (2014).

30. Dunn, K. E., Trefzer, M. A., Johnson, S. & Tyrrell, A. M. Investigating the dynamics of surface-immobilized DNA nanomachines. *Scientific Reports* **6**, 29581 (2016).

31. Mullor Ruiz, I. *et al.* Connecting localized dna strand displacement reactions. *Nanoscale* **7**, 12970–12978 (2015).

32. Gerasimova, Y. V. & Kolpashchikov, D. M. Towards a dna nanoprocessor: Reusable tile-integrated dna circuits. *Angewandte Chemie International Edition* **55**, 10244–10247 (2016).

33. Jung, J., Hyun, D. & Shin, Y. Physical synthesis of DNA circuits with spatially localized gates. In *33rd IEEE International Conference on Computer Design, ICCD 2015, New York City, NY, USA, October 18-21, 2015*, 259–265 (IEEE Computer Society, 2015).

34. Dirks, R. M. & Pierce, N. a. Triggered amplification by hybridization chain reaction. *Proceedings of the National Academy of Sciences of the United States of America* **101**, 15275–8 (2004).

35. Genot, A. J., Zhang, D. Y., Bath, J. & Turberfield, A. J. Remote toehold: A mechanism for flexible control of DNA hybridization kinetics. *Journal of the American Chemical Society* **133**, 2177–2182 (2011).

13

36. Lakin, M. R., Petersen, R. L., Gray, K. E. & Phillips, A. Abstract modelling of tethered DNA circuits. In *Lecture Notes in Computer Science*, vol. 8727, 132–147 (2014).

37. Chen, Y. J., Groves, B., Muscat, R. A. & Seelig, G. DNA nanotechnology from the test tube to the cell. *Nature Nanotechnology* **10**, 748–760 (2015).

38. Groves, B. *et al.* Computing in mammalian cells with nucleic acid strand exchange. *Nature Nanotechnology* 1–18 (2015).

39. Hemphill, J. & Deiters, A. DNA computation in mammalian cells: MicroRNA logic operations. *Journal of the American Chemical Society* **135**, 10512–10518 (2013).

40. He, Y. & Liu, D. R. Autonomous multistep organic synthesis in a single isothermal solution mediated by a DNA walker. *Nature Nanotechnology* **5**, 778–82 (2010).

41. Meng, W. *et al.* An autonomous molecular assembler for programmable chemical synthesis. *Nature Chemistry* **8**, 542–8 (2016).

42. Douglas, S. M., Bachelet, I. & Church, G. M. A logic-gated nanorobot for targeted transport of molecular payloads. *Science (New York, N.Y.)* **335**, 831–4 (2012).

43. Zadeh, J. *et al.* Nupack: Analysis and design of nucleic acid systems. *Journal of Computational Chemistry* **32**, 170–173 (2011).

314 **Author contributions**   G.C., N. D., R.M., A.P. and G.S. designed experiments and wrote the

315 paper. G.C. performed the experiments. N.D. and A.P. performed the modeling studies.

316 **Supplementary Materials**   Supplementary Information includes supplementary text, figures and
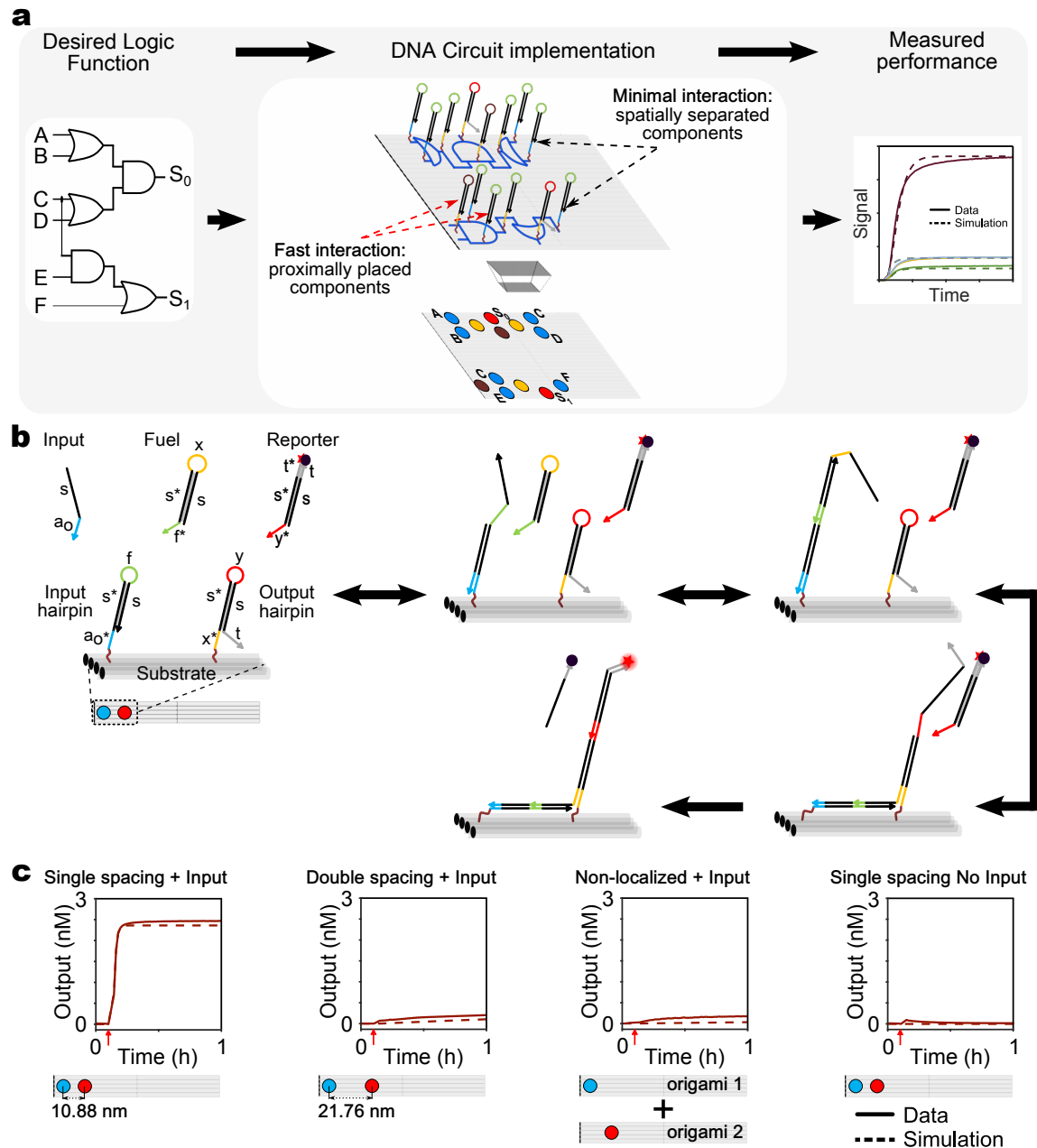
317 tables.

Figure 1: **Spatial organization controls signal propagation.** **a,** High-level abstraction of the circuit design process: An abstract logic circuit (left) is realized using DNA hairpin components arranged on a DNA origami (middle), tested experimentally and compared with model simulation (right). A top view of the localized circuit on origami (middle bottom panel) shows the four basic hairpins reused throughout all circuits in this paper as color-coded circles (Input hairpin (HP): blue; Intermediate hairpin: yellow; Output hairpin: red; Threshold hairpin: brown). **b,** Reaction mechanism for a two hairpin domino (2HP) wire. Arrows denote 3'-ends. Functional domains are indicated by color and labeled in the first panel (s: stem domain; a_0, x, f, y, t: toehold domains; s* represents a domain complementary to s). **c,** Unquenched fluorophore concentration plots (solid lines) and corresponding simulations (dashed lines) demonstrating signal transfer across localized and non-localized versions of a 2HP wire. **Left to Right:** Single-spaced 2HP wire; double-spaced 2HP wire; Input hairpin and Output hairpin on different origami; single-spaced 2HP wire without Input. Reactions were carried out at 25°C with 5 nM Origami, 40 nM Reporter, 100 nM Fuel, 50 nM Input in 1X TAE, 12.5 mM Mg^{++}. Red arrows indicate time points when input strands were added.
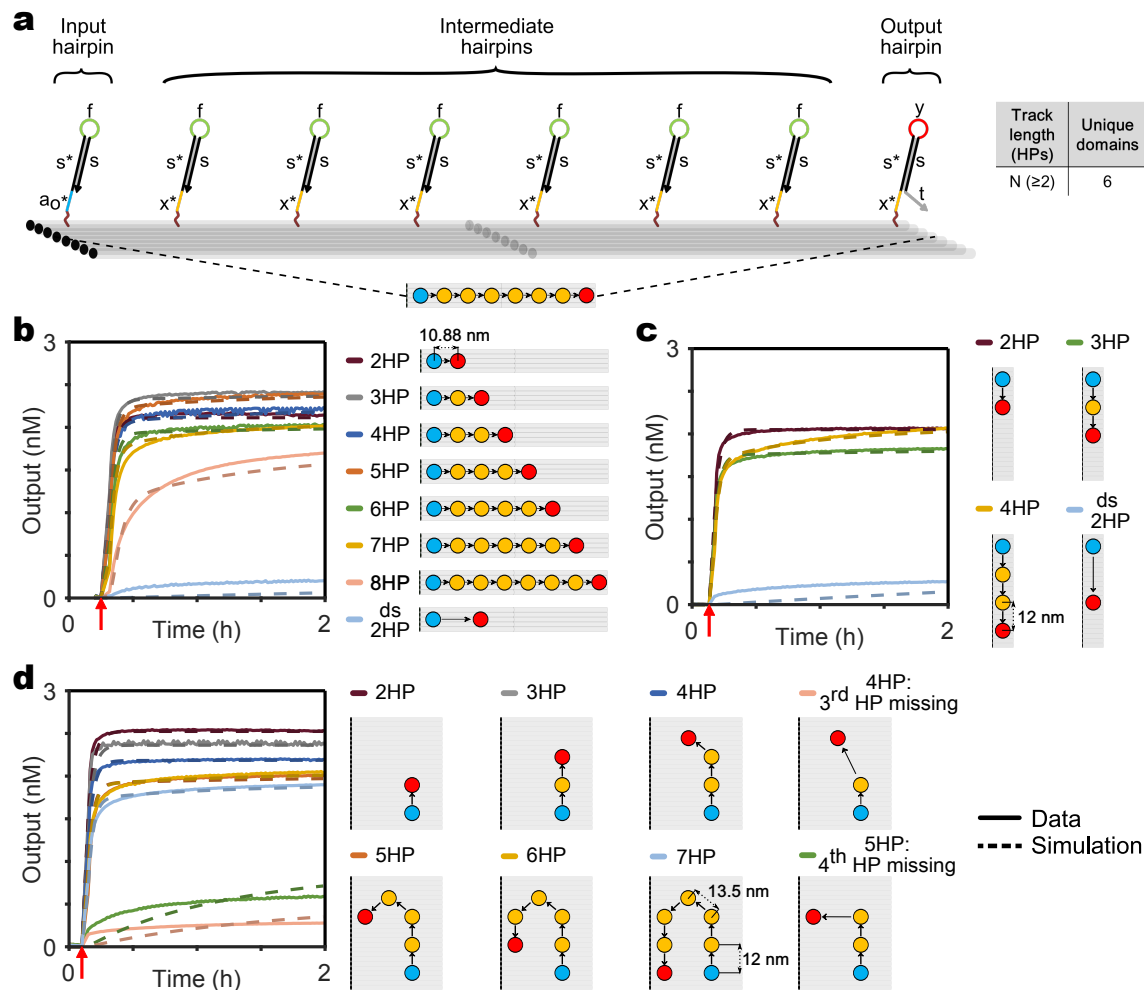
16

Figure 2: **Signals propagate along wires of different lengths and orientations. a,** Schematic representation of an untriggered eight hairpin (8HP) wire along the DNA origami helical axis (domains are labeled with lowercase letters). **Bottom panel:** Top view of the wire with Input hairpin (blue circle), six identical Intermediate hairpins (yellow circles) and Output hairpin (red circle). **Table:** Wires of arbitrary lengths can be built with only six unique domains. **b-d,** Signal propagation along the helical axis (b; 2-8 HP), perpendicular to the helical axis (c; 2-4 HP), and through a 180 degree turn (d; 2-7 HP). **Left:** Unquenched fluorophore concentration plots (solid lines) and simulations (dashed lines). Experimental conditions were as in Fig. 1. **Right:** Graphical depiction of all different wires. Hairpin spacing is consistent along the vertical (12 nm), horizontal (10.88 nm) and diagonal (13.5 nm) directions. Black arrows indicate the sequence of signal propagation. Red arrows indicate time points when inputs were added. ds 2HP represents a double-spaced two hairpin wire.
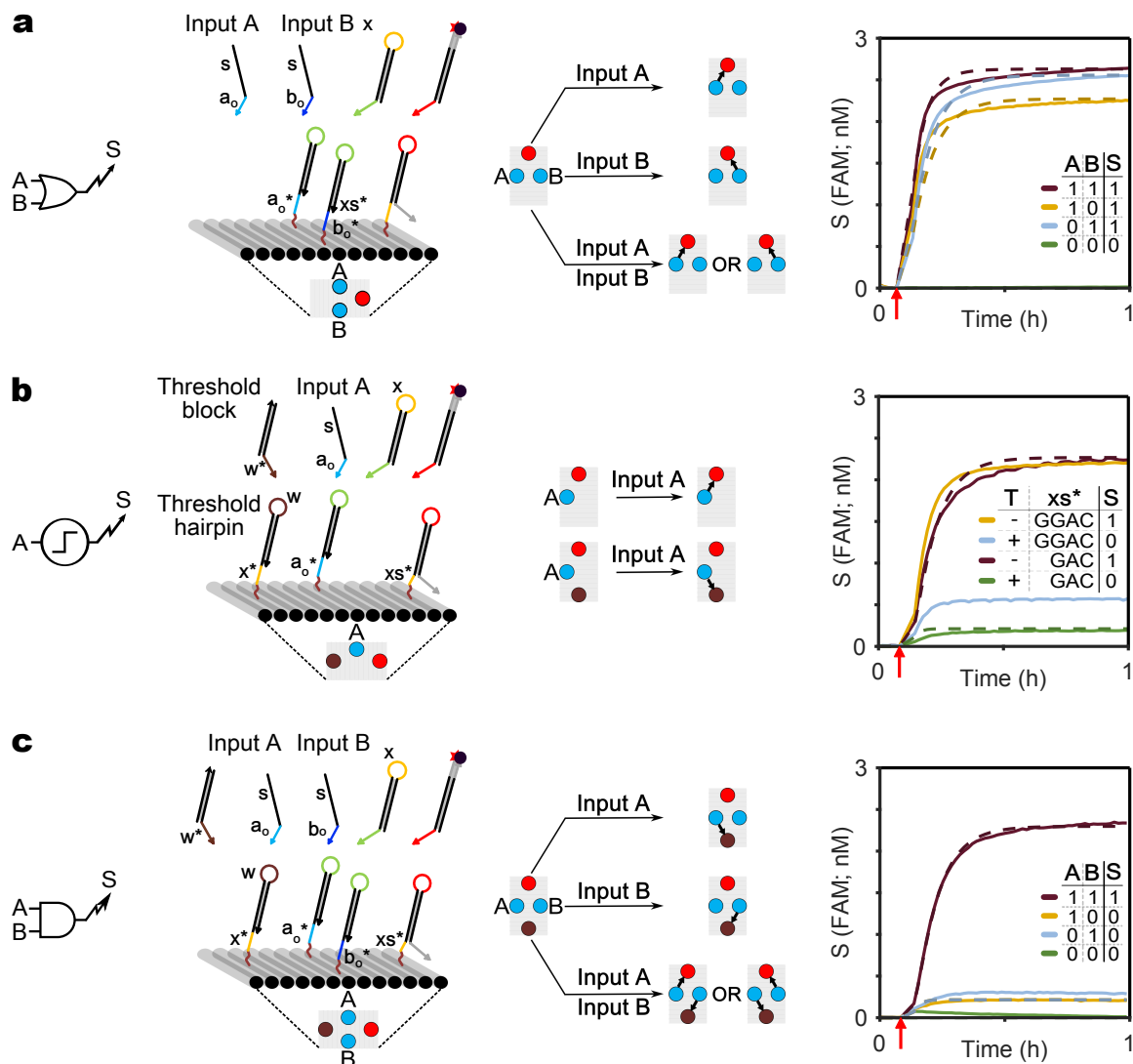
17

Figure 3: **Elementary logic gates are realized with localized DNA hairpins. a,** Two-input OR; **b,** Thresholding module; **c,** Two-input AND. **For (a-c), left:** Logic gate diagram. **second-to-left:** DNA domino representation and top view projection. All domains are labeled with lowercase letters and Inputs are distinguished by their toeholds (a_0 and b_0, blue). The output toehold domain xs* (yellow, 3 or 4nt) is a truncated version of x* (6nt). **second-to-right:** Graphical summary of circuit operation. For OR and AND gates, the response to different input combinations is depicted. For the threshold module, a circuit with a Threshold hairpin is compared to a circuit without it. Black arrows indicate the (most likely) direction of signal propagation. **right:** Unquenched fluorophore concentration plots (solid lines) and simulations (dashed lines). For AND and OR gates, legends are represented as truth tables, where presence of an input strand (A,B) or output signal (S) is denoted by "1" and their absence is denoted by "0". For the Threshold module, the T column indicates whether the system did (+) or did not (-) include the Threshold hairpin, which contains the x* domain (CTGGAC). The xs* column indicates whether the Output hairpin has a 3nt (GAC) or 4nt (GGAC) toehold. Experimental conditions were as in Fig. 1. Red arrows indicate when inputs were added.
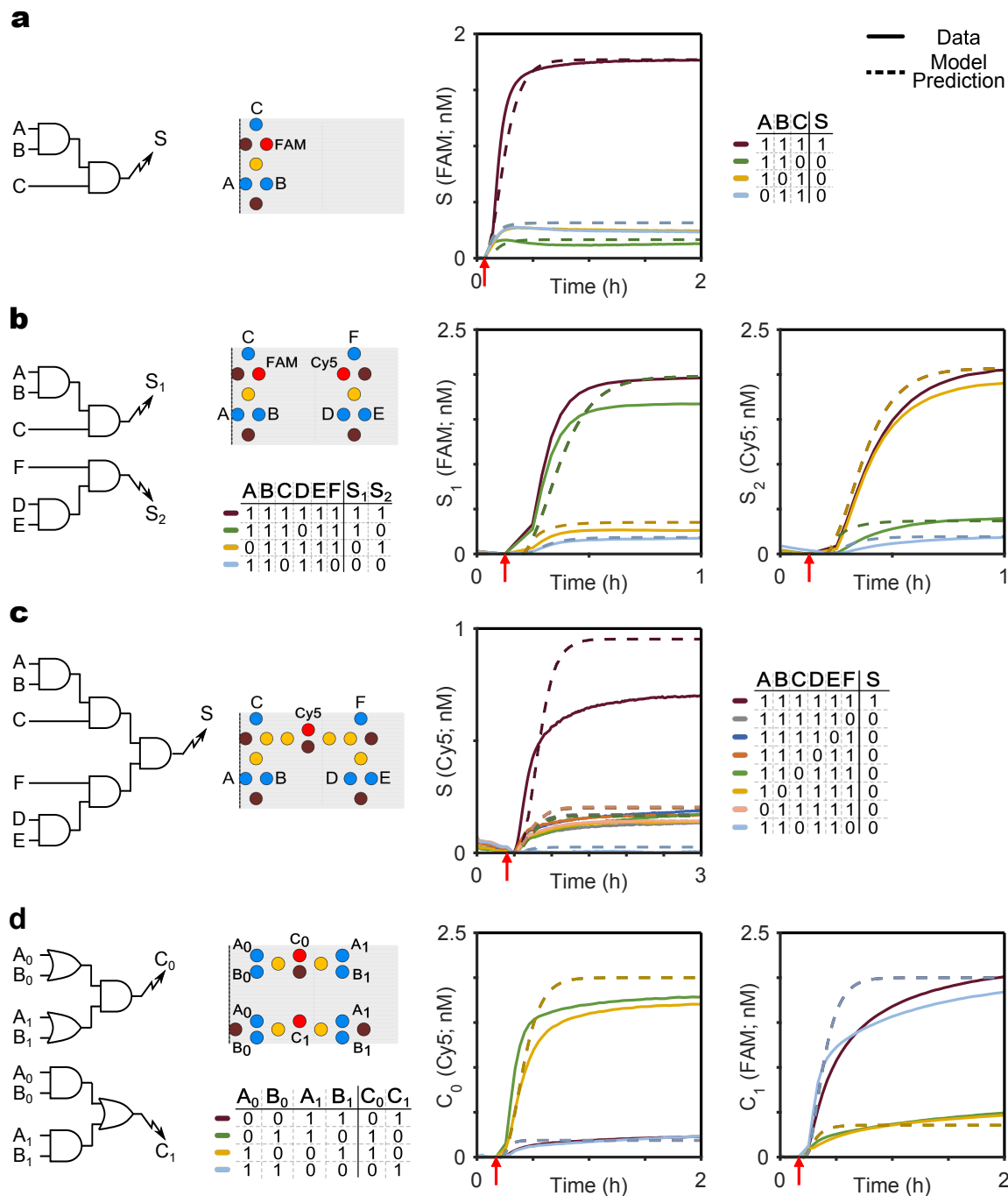
18

Figure 4: **Elementary logic gates are combined into multi-input logic circuits. a,** Three-input AND gate. **b,** Two three-input AND gates in parallel. **c,** Six-input AND gate. **d,** Two-input dual-rail XNOR gate. **left:** Logic circuit diagram. **middle:** Top view of the localized DNA circuit. **right:** Unquenched fluorophore concentration plots (solid lines) and model predictions (dashed lines). Legends are represented as truth tables, where presence of an input or Output is denoted by "1" and their absence is denoted by "0". Experimental conditions were as in Fig. 1. Red arrows indicate when inputs were added.

METHODS

319 **Component design.** All the hairpins used in this study were designed with a 12 nucleotide

320 stem to provide meta-stability while preventing any unnecessary loss of speed and chemical po-

321 tential due to branch migration through longer domains. The toehold domains were also chosen

322 to be 6 nucleotide long for optimal strand displacement speed. The domino wires were built with

323 three basic components: Input hairpin, Intermediate hairpin and Output hairpin. In addition, the

324 freely floating components: Input strand, Fuel complex and Reporter complex interacted with the

325 localized components to propagate the signal (Fig. 1b). For designing a wire of any length, five

326 unique 6 nucleotide domains (a_0, f, x, y, t) and one 12 nucleotide long domain (s) were designed.

327 All the circuit components use a combination of these six domains as specified in Fig. 1b. For

328 designing the 2-Input AND domino gate, one more domain (w) was required for the hairpin loop

329 of Threshold hairpin. The Reporter complex was designed to have an 18 nucleotide long double

330 stranded stem to aid towards its stability at 25°C. Accordingly the Output hairpin was designed

331 to have 6 nucleotide 3'-flanking domain (t). For designing logic circuits with multiple inputs and

332 outputs, Input hairpins with orthogonal 5'-toehold domains (a_0,b_0,c_0,d_0,e_0,f_0) and Output hairpins

333 with orthogonal hairpin loops (y, y2) were designed. The 3'-flanking domains (grey domains)

334 in the Output hairpins were different for the wires (t) and logic circuits (t2). All the other com-

335 ponents in the logic circuits were similar to those used for signal transmission lines. For each

336 localized hairpin at a particular position on the origami, the sequence of the origami staple with its

337 3'-end at that position was extended with the sequence of corresponding hairpin along its 3'-end

338 by a 5 nucleotide polyT linker. The linkers provided conformational flexibility to the hairpins, thus

339 aiding signal propagation on the origami scaffold.

340   **Sequence selection.**   NUPACK [43] was used to generate a set of orthogonal 6 nucleotide

341 toeholds and 12 nucleotide stem domains. No more than 3 G's, C's, A's or T's were allowed con-

342 secutively and the ensemble defect was set to 1 percent. For different circuits, corresponding num-

343 ber of domains were selected from the master pool to generate individual component sequences.

344 These sequences were then verified by NUPACK to detect possible non-intended interactions and

345 the domains were further optimized if any significant interaction was detected.

346   **Preparation of a localized circuit.**   We used a twist-corrected version of the rectangular

347 tile origami[8] as a scaffold for our study. Twist-correction by base deletion at every third turn on

348 the helical axes has been shown to reduce global twist, thus providing greater predictability in

349 circuit design and improved assembly. We didn't add any edge staples to prevent origami edge

350 stacking while annealing [8]. For origami preparation, standard desalted DNA staple strands were

351 batch ordered in 96 well plates at stock concentrations of 400 μM in RNase-free water from Inte-

352 grated DNA Technologies (IDT) and m13mp18 single stranded template DNA was ordered from

353 Bayou Biolabs. Modified staple strands with component hairpin sequences at the 3'-end, Fuel com-

354 plex, Input strands, and Fluorophore-labeled and quencher labeled strands for different Reporter

355 complexes were ordered with HPLC purification from IDT. In addition, for each Output hairpin, an

356 Output opening strand (OOS): complementary to the 5'-toehold and the adjacent stem domain; and

357 for each Reporter complex, a Reporter opening strand (PO): complementary to the fluorophore-

358 labeled strand, was ordered with HPLC purification from IDT and the lyophilized samples were

359 re-suspended with Tris-EDTA buffer (TE: Nuclease free, pH 8.0) to stock concentrations of 100

360 μM and stored at -20°C. Diluted aliquots were further prepared for each of the hairpin staples, the

361 corresponding unmodified staples and other strands as and when needed for regular use, and were

362 stored temporarily at 4°C. Three master layouts were prepared with the origami scaffold: one for

363 the wires (Supplementary Information Fig. S1a), one for the logic circuits (excluding dual rail

21

364 XNOR) (Supplementary Information Fig. S1b), and one for the dual rail two-input XNOR circuit

365 (Supplementary Information Fig. S1c). All the circuit operations explained in the study were per-

366 formed using subsets of these three blueprints. For each blueprint, 4 μM master stocks (one each

367 for top half and bottom half of the origami) of staples were prepared excluding the staples in the

368 blueprint. For preparing a specific wire or logic gate , 1X m13mp18 template DNA was mixed

369 with 5X of the staple master stocks, 10X of the corresponding modified staples with hairpins and

370 10X of unmodified staples for the rest of the sites for that blueprint. These components were com-

371 bined in Tris-Acetate EDTA buffer with 12.5 mM Mg^{++} (1X TAE/Mg^{++}: 40 mM Tris base, 20

372 mM acetic acid, 2 mM EDTA and 12.5 mM magnesium acetate, adjusted to pH 8.0); 1X = 60 nM.

373 The reaction mix was then annealed by incubation at 95°C for 2 minutes, slow cooling to 60°C at

374 0.1°C every 12 seconds, incubation at 60°C for 12 minutes, slow cooling to 25°C at 0.1°C every

375 12 seconds, and hold at 4°C for up to 24 hours (Annealing Protocol 1).

376   Stock solutions of 10 μM Fuel complex was prepared in 1X TAE/Mg^{++} and was annealed by

377 heating it to 95°C for 2 minutes and slowly cooling to room temperature at 0.1°C every 6 seconds

378 (Annealing Protocol 2). The Reporter complexes were annealed following Annealing Protocol 2

379 after mixing fluorophore-labeled strand and quencher-labeled strand at molar ratios of 1:1.2 in 1X

380 TAE/Mg^{++}.

381   **Purification of circuit components.** Annealed origamis were purified to remove excess

382 staple strands through size exclusion chromatography using Sephacryl S300-HR resin (GE Health-

383 care Life Sciences). The Sephacryl S300-HR resin is commercially pre-equilibrated in 20% ethanol.

384 Aliquots of Sephacryl S300-HR were collected in 50 ml falcon tubes and centrifuged at 1000 g for

385 5 minutes in 4°C. The supernatants containing ethanol were discarded and the resin pellets were

386 equilibrated three times with distilled water and three times with 1X TAE/Mg^{++} by re-suspending

387 the pellets with solvents to 50 ml by shaking, centrifugation at 1000 g for 5 minutes in 4°C, and

388 discarding the supernatants. After the supernatants were discarded in the final round, the resin

389 pellets were re-suspended with equal volumes of 1X TAE/Mg^{++} and stored at 4°C. For preparing

390 each size-exclusion column, 500 μl of re-suspended resin was added to 0.8 ml Micro Bio-Spin^{TM}

391 Chromatography column (Bio-Rad Laboratories) with collection tube and centrifuged at 1000 g

392 for 5 minutes in room temperature. The flow-through was discarded and an additional 500 μl

393 of resin was added to the column before another centrifugation at 1000 g for 5 minutes at room

394 temperature. Three such columns were prepared for purification of up to 50 μl of each origami

395 construct. The resultant columns were placed on fresh sterile 1.7 ml Eppendorf tubes and up to 50

396 μl of annealed origami was loaded on each column for the 1st round of purification. Each column

397 was centrifuged at 1000 g for 5 minutes at room temperature, and the flow-through was collected

398 and loaded onto a fresh column for the 2nd round of centrifugation. After repeating the process

399 through a 3rd round, the flow-through for each origami sample was collected for experiments. Sup-

400 plementary Information Fig. S2 shows a 1% Agarose Gel analysis demonstrating the efficiency of

401 the purification protocol. We observe minimal loss of origami with almost complete purification

402 of any excess staples after three rounds of purification.

403 For the domino wires, the annealed Reporter complex was further run through 10% Poly-

404 acrylamide gel electrophoresis (PAGE) with 12% glycerol as loading agent, to remove the excess

405 quencher-labeled strand. The band corresponding to the full Reporter Complex was visualized

406 using black light and cut out and suspended in 1X TAE/Mg^{++} for 24 hours at room temperature.

407 The resultant solvent was extracted and stored at 4°C for kinetics experiments.

408 **Fluorescence kinetics experiments.** Kinetics experiments were performed on a spectroflu-

409 orometer (Horiba Scientific: Fluorolog®-3 and FluoroMax®-4) with 0.875 ml Fluorometer Micro

410 Square Cells with polytetrafluoroethylene (PTFE) stoppers (Starna: 23-5.45-S0G-5) and cuvette

411 adaptors (Starna: FCA5). A maximum of four samples were tested for each set of measurements

412 using a 5 nm slit width for both excitation and emission monochromators and an integration time

413 of 10 seconds. Excitation and emission wavelengths of different fluorophores used in various ex-

414 periments were as follows: FAM (495 nm / 520 nm), Cy5 (648 nm / 668 nm). For experiments

415 using a single Reporter, measurements were taken every 60 seconds, while for experiments using

416 two Reporters, measurements were taken every 120 or 150 seconds. Before an experiment, the

417 cuvettes were cleaned by washing 5 times with distilled water, once with 70% ethanol, and another

418 5 times with distilled water. The excess residual water was dried out of the cuvettes with airflow.

419 Then, generally all the circuit components except the Input strand(s) were mixed and added to the

420 cuvettes and an initial steady state signal for each sample was measured as baseline. After that, the

421 experiment was paused, for addition of Input strand(s) and subsequent mixing by gentle vortex or

422 inverted shaking. The cuvettes were then put back to the fluorometer, before the experiment was

423 resumed. After the completion of data collection for circuit performance, an excess (400 nM) of

424 corresponding OOS was added to trigger the unreacted Output hairpin. The resultant final output

425 signal was representative of the total number of output hairpins and was taken as a close approxi-

426 mation of the total number of origami molecules present in the solution for modeling studies.

427 **Data representation.** Arbitrary fluorescence units (S/R values) obtained from the spec-

428 trophotometer were converted to the concentrations of the corresponding unquenched fluorophore

429 strands using a calibration curve of each Reporter complex. Because we observed small variations

430 in fluorescence signal between different cuvette positions, calibrations were performed for each

431 position independently. To construct a calibration curve, a pre-determined volume of annealed

432 Reporter complex stock was re-suspended in 1X TAE/Mg^{++}, added to the cuvette and an initial

433 baseline signal was recorded for each cuvette. That was followed by stepwise addition of known

434 concentrations of Reporter triggering PO strands. After each trigger strand addition, the increase

435 in signal was recorded till a steady state value was reached. The baseline-corrected signal values

24

were then plotted against the PO strand concentrations to obtain a calibration curve. The signal values were linearly proportional to the fluorophore concentrations and the slope of a linear fit was recorded as the signal-to-concentration "conversion factor" for that cuvette position and Reporter. Supplementary Information Fig. S3 shows an example calibration curve for one of the Reporters used in this study.

Finally, an excess of PO strand was added to the solution to trigger all the Reporter complexes, and the final increase in signal was divided by the conversion factor to get the actual concentration of the Reporter complex in the solution, and in turn the actual concentration of the Reporter complex stock. Importantly, these conversion factors were used to translate the increase in output signal due to signal propagation through a circuit using the corresponding Reporter complex as output. Fresh calibration curves were constructed on event of a change in external experimental conditions like different cuvettes, new xenon lamp, different batch of Reporter strands, etc. to maintain accuracy and consistency across different experiments.

Agarose and polyacrylamide gel electrophoresis (PAGE). For analyzing the purification efficiency using Sephacryl S300-HR resin purification method, 1% Agarose gel was prepared by mixing 1 g of Ultrapure TM Agarose (Thermo Fisher Scientific; Catalog#: 16500500) in 100 ml of 1X TAE/Mg^{++}. The solution was then heated to boil and cooled down to 50-60°C to dissolve the Agarose before pouring it to the gel tray to solidify the gel. The solidified gel was placed in the gel tray in a container with ice such that the side and bottom walls of the gel tray are always in contact with ice. Pre-cooled 1X TAE/Mg^{++} was added as running buffer till the gel was completely submerged in the tray. This prevents over-heating of the gel and the buffer and minimizes dissociation of the origamis while running the gel. Origami samples were mixed with appropriate volumes of 80% glycerol to achieve final concentrations of 12% glycerol by volume, which acted as a loading agent. The gel was then run at 100 V for 1 hour and stained with SYBR Gold (Thermo Fisher

25

460 Scientific; Catalog No.: S11494) for 15 minutes before imaging. Gel Imaging was performed us-

461 ing Typhoon FLA 9000 Gel Imaging Scanner (GE Healthcare Life Sciences) at 50 μm resolution

462 using the SYBR Gold Nucleic Acid stain filter settings. For purifying the Reporter complex used

463 in signal transmission experiments with wires, 10% Polyacrylamide gel was prepared by mixing

464 5 ml 19:1 40% acrylamide/bis, 2 ml 10X TBE/Mg^{++}, and deionized water to 20 ml. Then 150 μl

465 APS and 15 μl TEMED were added to accelerate the polymerization of acrylamide. Annealed Re-

466 porter complexes were mixed with 80% Glycerol to achieve final concentrations of 12% glycerol

467 by volume and loaded to the wells of the gel (upto 60 μl of sample per well). PAGE gels were run

468 in 1X TBE/Mg^{++} at 120 V for 40 minutes to separate the excess quencher-labeled strands from the

469 annealed Reporter complexes and then the Reporter complexes were extracted as described before.